Dalton Transactions

PERSPECTIVE

View Article Online
View Journal

Cite this: DOI: 10.1039/c9dt00491b

A look at periodic trends in d-block molecular electrocatalysts for CO_2 reduction

Changcheng Jiang, Asa W. Nichols and Charles W. Machan *

Received 1st February 2019,
Accepted 9th April 2019

DOI: 10.1039/c9dt00491b

rsc.li/dalton

Electrocatalytic CO_2 reduction is of continued interest to sustainable energy research. Mononuclear transition metal complexes from Group 6 to Group 10 with a select subset of ligand frameworks have been demonstrated to be efficient electrochemical CO_2 reduction catalysts. Here, we review the known mononuclear complexes from Group 6 to Group 10, examining trends in activity, electronic structure of catalytic intermediates, and product selectivity. The correlation between differences in electronic structure and CO_2 reduction activity between these metal centers are discussed.

1. Introduction

The rising concentration of carbon dioxide (CO_2) in the atmosphere from anthropogenic sources is widely acknowledged to be a major contributor to global climate change.[1–3] Annually, ~30 billion tons of carbon dioxide are produced by burning fossil fuels to fulfill energy needs for power generation, transportation, heating, and industry.[4] Using electrochemical routes to convert CO_2 to valuable commodity chemicals like CO, formic acid (HCOOH), methanol (CH_3OH), *etc.*, is an attractive strategy to manage the related environmental effects as a substitute for non-renewable hydrocarbon feedstocks.

One of the biggest obstacles for the large-scale electrochemical reduction of CO_2 is finding low-cost and efficient electrocatalysts. Since the 1980s, a significant number of molecular complexes, based on transition metals ranging from Group 6 to Group 10, have been reported with high activity for electrochemical CO_2 reduction.[5–8] Early reports focused on precious metal complexes such as $[Ru(bpy)_2(CO)_2]^{2+}$, *fac*-[Re(bpy)$(CO)_3$Cl] and $[Pd(triphos)(MeCN)]^{2+}$.[9–11] A few 3d metal complexes with macrocyclic ligands such as [Fe(TPP)Cl] and $[Ni(cyclam)]^{2+}$ were also discovered around the same time.[12–15]

To date, many transition metal complexes from Group 6 to Group 10 have been observed with electrochemical CO_2 reduction activity. Among them, Tc is the only one without any detailed study, owing to its radioactive instability. Complexes based on Mn,[16–18] Fe,[19–21] Co,[22–24] Ni,[25–29] Ru,[30–32] Pd,[33,34] Re[35–37] and Ir[38–40] have received most of the attention and often show electrochemical CO_2 reduction activity with multiple ligand systems. In comparison, Cr,[41] Mo,[42,43] Rh,[44] W,[42,43] Os[45] and Pt[46,47] have fewer or limited positive reports. Interestingly, most recent research focuses on 3d metal-based electrocatalysts (Mn, Fe, Co and Ni), which have shown equivalent or higher activity with respect to their 4d/5d analogues.[25,48,49]

The general developments in electrochemical CO_2 reduction with homogenous catalysts have been covered in several recent reviews.[8,50,51] Here, we look at transition metal complexes from Group 6 to Group 10 capable of electrocatalytic CO_2 reduction, focusing exclusively on mononuclear complexes. Despite the extensive involvement of redox non-innocent ligands and strong secondary-sphere effects, the underlying influence of periodic electronic structure changes across these metal centers is apparent.

2. Electrochemical CO_2 reduction with transition metal complexes

2.1 Homogeneous electrocatalysts

Homogenous molecular electrocatalysts work differently from heterogeneous electrocatalysts because the electrode does not participate in the catalytic reaction directly.[48] In electrocatalytic CO_2 reduction with homogenous catalysts, the catalytic reactions are conducted by active species generated by heterogeneous electron transfer from the electrode, as shown in Fig. 1A. The active catalyst species can then react with substrate molecules in solution in a diffusion-limited process. Due to inherent mass transfer restrictions, electrocatalytic CO_2 reduction takes place only within a thin layer adjacent to the electrode as shown in Fig. 1B.

An electrochemical reaction on an electrode generally operates at an overpotential (η), which is the difference between the standard potential of a reaction of interest and the potential applied to the electrode to drive the reaction. Since CO_2 is a relatively inert molecule, direct electrochemical CO_2 reduction

Department of Chemistry, University of Virginia, PO Box 400319, Charlottesville, VA 22904-4319, USA. E-mail: machan@virginia.edu

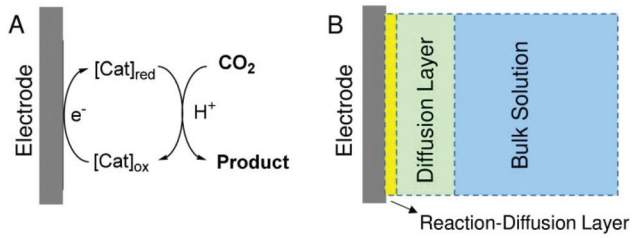

Fig. 1 Schematic representation of (A) CO_2 reduction with homogenous electrocatalysts and (B) layered solution structure on electrode at steady state.[6,52]

comes with a large energy penalty and the single-electron reduction of CO_2 to form $CO_2^{\bullet-}$ occurs at −1.9 V *vs.* NHE.[53] Proton-coupled CO_2 reduction can significantly reduce the standard reduction potential for multielectron CO_2 reduction as shown in Table 1. However, there are significant kinetic challenges to mediating several electron transfer (ET) and proton transfer (PT) reactions concurrently or consecutively.[54,55]

Table 1 Standard Potentials for CO_2 Reduction in Aqueous Solutions at pH 7.[6,56]

ET/PT	Reaction	Potential (V *vs.* NHE)
$1e^-$	$CO_2 + e^- \rightarrow CO_2^{\bullet-}$	−1.90
$2e^-/2H^+$	$CO_2 + 2e^- + 2H^+ \rightarrow CO + H_2O$	−0.53
	$CO_2 + 2e^- + 2H^+ \rightarrow HCOOH$	−0.61
	$2CO_2 + 2e^- + 2H^+ \rightarrow H_2C_2O_4$	−0.54
$4e^-/4H^+$	$CO_2 + 4H^+ + 4e^- \rightarrow CH_2O + H_2O$	−0.48
$6e^-/6H^+$	$CO_2 + 6H^+ + 6e^- \rightarrow CH_3OH + H_2O$	−0.38
$8e^-/8H^+$	$CO_2 + 8H^+ + 8e^- \rightarrow CH_4 + 2H_2O$	−0.24

Transition metal complexes can function as catalysts to promote the reduction of CO_2 and reduce the overpotential with mediated electron transfer and proton transfer. We have selected representative molecular electrocatalysts of CO_2 reduction for each of the known metal centers from Group 6 to Group 10, shown in Fig. 2. The chosen catalysts have received relatively intensive study and are helpful to analyze and compare the role of the metal centers in the observed activity.

Most frequently, electrocatalytic CO_2 reduction with transition metal catalysts generates the $2e^-$ reduction products like CO and formic acid/formate ($HCOOH/HCOO^-$) (H_2 is often a side product for CO_2 reduction either from hydrogen evolution reaction (HER) activity of the electrocatalyst or the electrode).

Turnover frequency (TOF, more often TOF_{max}) and Faradaic efficiency (FE) are used to quantify the activity and selectivity of molecular electrocatalysts. Well-established electrochemical methods like cyclic voltammetry (CV) and controlled potential electrolysis (CPE) are commonly used to obtain these parameters.[52,57,58] The performances of the selected electrocatalysts in Fig. 2 are summarized in Table 2. The catalytic rates of these molecular electrocatalysts, as quantified by TOF_{max}, range from a few turnovers per second to tens of thousands of turnovers per second. There are very selective electrocatalysts that produce a single product like *fac*-Mn(^{t}Bu-bpy)(CO)$_3$Br (CO) and $[Ir(POCOP)(MeCN)_2H]^+$ (HCOOH/$HCOO^-$), but others are considerably less selective and produce a mixture of products, like $[Co(N_4H)(Br)_2]^+$ (CO and H_2).

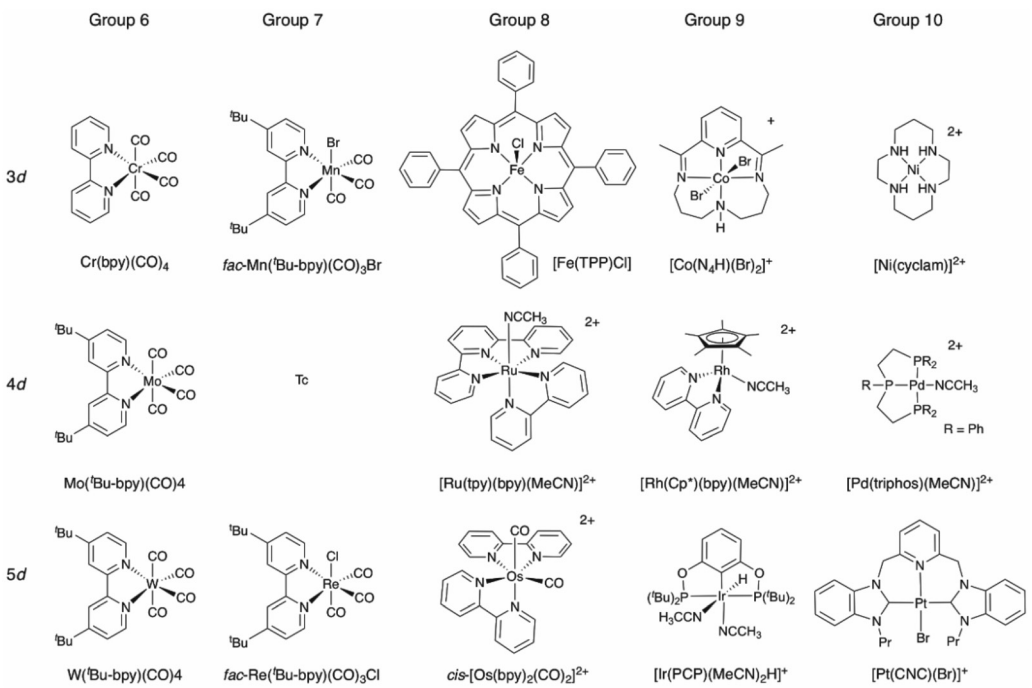

Fig. 2 Selected mononuclear d-block catalysts for electrocatalytic CO_2 reduction.

Table 2 Summary of selected mononuclear CO_2 reduction catalysts in d-block: oxidation state involved, conditions, products and activity

	Electrocatalyst[s]	Active species for CO_2 binding[a]	Oxidation states of metal center in catalytic cycle	CPE conditions: solvents, proton source, electrode, potential (V)	Products[b] (FE in %)	TOF_{max} [c]	Ref.
3d	$Cr(bpy)(CO)_4$	$[Cr(0)(bpy^{\bullet\bullet})(CO)_3]^{2-}$	Cr(0)	—	—	N.A.	41
	fac-$Mn(^tBu\text{-}bpy)(CO)_3Br$	$[Mn(0)(bpy^{\bullet})(CO)_3]^{-}$	Mn(0), Mn(I)	MeCN, TFE, GC electrode, −2.0 V *vs.* SCE	CO (100)	340 s^{-1}	16, 17, 60 and 61
	[Fe(TPP)Cl]	$[Fe(0)(TPP)]^{2-}$	Fe(0), Fe(I), Fe(II)	DMF, phenol, Hg pool, −1.70 V *vs.* SCE	CO (94)	5.8×10^4 s^{-1}	12 and 54
	$[Co(N_4H)(Br)_2]^{+}$	$[Co(0)(N_4H)]$	Co(0), Co(I)	MeCN, H_2O, GC electrode, −2.13 V *vs.* Fc^{+}/Fc	CO (45) H_2 (30)	N.A.	24
	$[Ni(cyclam)]^{2+}$	$[Ni(I)(cyclam)]^{+}$	Ni(I), Ni(II)	MeCN, H_2O, GC electrode, −1.45 V *vs.* SCE	CO (90)	90 s^{-1}	13, 26 and 62
4d	$Mo(^tBu\text{-}bpy)(CO)_4$	$[Mo(0)(bpy^{\bullet\bullet})(CO)_3]^{2-}$	Mo(0)	MeCN, GC electrode, −2.3 V *vs.* SCE	CO (109)	1.9 s^{-1}	42
	Tc	—	—	—	—	—	—
	$[Ru(tpy)(bpy)(MeCN)]^{2+}$	$[Ru(II)(tpy^{\bullet})(bpy^{\bullet})(MeCN)]$	Ru(II), Ru(I)	MeCN, GC electrode, −1.52 V *vs.* NHE	CO (76)	5.5 s^{-1}	30, 32 and 63
	$[Rh(Cp^*)(bpy)Cl]^{+}$	$[Rh(III)(Cp^*)(bpy)H]^{+}$	Rh(I), Rh(III), Rh(II)	MeCN, H_2O, GC electrode, −2.0 V *vs.* SCE	$HCOO^{-}$ (49) H_2 (16)	N.A.	64
	$[Pd(triphos)(MeCN)]^{2+}$	$[Pd(triphos)(MeCN)]^{+}$	Pd(I) Pd(II)	MeCN, H_2O, GC electrode, −2.0 V *vs.* SCE	CO (85) H_2 (16)	12 s^{-1}	65–67
5d	$W(^tBu\text{-}bpy)(CO)_4$	$[W(0)(bpy^{\bullet\bullet})(CO)_3]^{2-}$	W(0)	—	—	2.2 s^{-1}	42
	fac-$Re(^tBu\text{-}bpy)(CO)_3Cl$	$[Re(0)(bpy^{\bullet\bullet})(CO)_3]^{2-}$	Re(0), Re(I),	MeCN, TFE, GC electrode, −2.0 V *vs.* SCE	CO (99)	570 s^{-1}	35 and 68–70
	cis-$[Os(bpy)_2(CO)H]^{+}$	*cis*-$[Os(0)(bpy)(bpy^{\bullet})(CO)H]^{-}$	Os(0), Os(II)	MeCN, H_2O, GC electrode, −1.4 V *vs.* SCE	CO (47) $HCOO^{-}$ (3)	4.9 s^{-1}	45
	$[Ir(PCP)(MeCN)_2H]^{+}$	$[Ir(III)(PCP)H_2]$	Ir(I), Ir(III)	MeCN, H_2O, GC electrode −1.45 V *vs.* NHE	$HCOO^{-}$ (85) H_2 (15)	20 s^{-1}	39 and 71
	$[Pt(CNC)(Br)]^{+}$	$[Pt(I)(CNC^{\bullet})(Br)]^{+}$	Pt(I), Pt(II)	DMF, TFE, GC electrode −2.25 V *vs.* Fc^{+}/Fc	CO (4)	N.A.	46

[a] Ligands are abbreviated for clarity, $^{\bullet}$ indicates a ligand-centered radical. [b] Hydrogen (H_2) is often generated as side product of electrochemical CO_2 reduction either from HER activity of the electrode or the metal complexes acting as HER catalyst in the presence of proton source. [c] TOF_{max} presented here are just qualitative indicators for the activity of the catalyst and they depend on the experimental conditions like substrate concentrations. TOF_{max} of Fe, Ru, Pd, Ir are generated based on reported catalytic rate constants reported from CVs. GC = glassy carbon.

It is important to note that the listed complexes in Fig. 2 are not necessarily able to react with CO_2 directly, instead requiring electrochemically reducing conditions: they are best described as "pre-catalysts".[48] Besides catalytic activity and product selectivity, Table 2 also summarizes proposed active species and proposed redox assignments for the metal center and ligand during the catalytic cycle. The formal charges of the metal centers and ligands in these active intermediates were adopted generally based on conventions and the most recent studies.[8,59]

We acknowledge that there are continued debates for oxidation number assignments and the nature of the intermediates.[72–74] Although the use of oxidation states is a simplification (molecular orbitals involve metal and ligand contributions with electron density distributed on a continuum), the simplification is nonetheless useful to rationalize their reactivity toward substrate molecules like CO_2 and H^+.[75]

2.2 CO_2 Reduction mechanism and products

The most common proton-assisted catalytic CO_2 reduction involving transition metal electrocatalysts result in $2e^-$ reduction products like CO and $HCOOH/HCOO^-$. The selectivity originates from the CO_2 activation pathways as shown in Scheme 1. In general, CO_2 can be activated directly by a reduced metal center to form a CO_2 adduct, $M(CO_2)$ as shown in Scheme 1-1. Alternatively, CO_2 could be activated by a metal hydride if the reduced metal complex prefers to react with a H^+ donor first, as shown in Scheme 1-2.

Although the exact binding mode of the CO_2 adduct $M(CO_2)$ is often not reported in electrocatalysts studies,[77] the reductive activation of CO_2 by low-valent transition metal complexes has been studied for decades.[78–80] The hydroxycarbonyl-type intermediate $M(\eta^1\text{-COOH})$, generated by protonation of $M(CO_2)$, has been identified as the key intermediate to electrocatalytic CO_2 reduction to CO and H_2O.[76,81] *Nota bene*, under aprotic conditions, CO_2 itself can become a suitable oxygen acceptor to form carbonate as a co-product. The reaction between CO_2 and a M–H bond generally forms metal formato type intermediates, $M(\eta^1\text{-OCOH})$ and leads to the generation of formic acid/formate.[8]

The formation of metal-bound carbonyl species from $M(\eta^1\text{-COOH})$ intermediates *via* C–O bond cleavage has been observed experimentally with ruthenium polypyridyl complexes, $[Ru(bpy)_2(CO)_2]^{2+}$, which was studied extensively by Tanaka and coworkers.[9,82,83] As shown in Fig. 3, spectroscopic studies on $[Ru(bpy)_2(CO)_2]^{2+}$ revealed fast, pH-dependent equilibria between three species: the $\eta^1\text{-}CO_2$ adduct $[Ru(bpy)_2(CO)(\eta^1\text{-}CO_2)]$, the hydroxycarbonyl $[Ru(bpy)_2(CO)(\eta^1\text{-COOH})]^+$, and the CO adduct $[Ru(bpy)_2(CO)_2]^{2+}$. The conversion of $M(\eta^1\text{-COOH})$ to the carbonyl species by hydroxide elimination or protonation is representative of the possible reaction pathways during the electrocatalytic CO_2 reduction to CO.

The production of $HCOOH/HCOO^-$ from the formato type intermediate with further protonation is much easier to visualize.[84] $HCOOH/HCOO^-$ are the most common CO_2 reduction products when activation proceeds through the metal hydride. Nevertheless, isomerization from $M(\eta^1\text{-OCOH})$ to $M(\eta^1\text{-COOH})$ is proposed to occur in a few cases.[31,85,86] There are no clear-cut demonstrations of CO_2 insertion into a M–H bond to generate the hydroxycarbonyl species $M(\eta^1\text{-COOH})$, although the reverse reaction is known to occur.[76]

2.3 Role of sacrificial proton source

Commonly, CO_2 reduction tests are carried out in polar aprotic solvents, especially acetonitrile (MeCN) and *N*,*N*-dimethylformamide (*N*,*N*-DMF), with proton sources added for enhanced product formation. Water is a convenient solvent and proton source for CO_2 reduction, but often is only used in mixed solvent systems. There are select cases where molecular electrocatalysts for CO_2 reduction are functional in pure water.[19,20,39,87] Like all coordinating solvents, water has potential inhibitory effects for CO_2 binding due to competitive

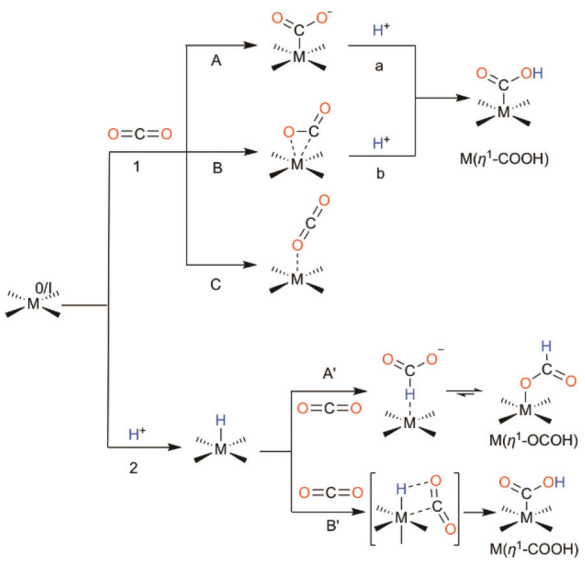

Scheme 1 CO_2 activation pathways by reduced transition metal complexes and metal hydrides.[76]

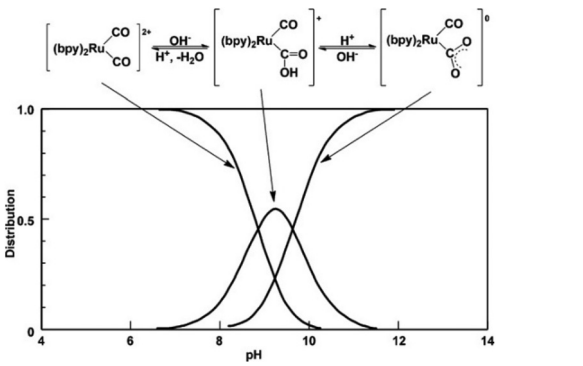

Fig. 3 CO formation from hydroxycarbonyl intermediate exemplified by equilibria of the ruthenium species in H_2O at various pH. Adapted with permission from *Inorg. Chem.*, 2015, **54**, 5085–5095. Copyright 2015, American Chemical Society.[82]

coordination at the catalyst center.[88] The solubility of transition metal complexes in water is also a prominent issue, requiring synthetic solutions.

Weak Brønsted acids such as methanol (MeOH), 2,2,2-trifluoroethanol (TFE), and phenol (PhOH) have been utilized as alternative proton donors and have shown increased catalytic activity and lifetime.[12,89] Proton donor activity is important to modulate the CO_2 reduction activity and can be used to tune the overpotential for the pK_a-dependent CO_2 reduction reaction.[90] The formation of a hydrogen bond with bound CO_2 can also facilitate binding to the metal center.[72] Generally, the inclusion of an appropriate proton source reduces overpotential by favoring concerted electron and proton transfer steps (such as PCET, proton coupled electron transfer) during CO_2 reduction.[70,91] However, proton sources of sufficient activity can also shift the reaction pathway towards the thermodynamically favored HER reaction.

2.4 Periodic trends and redox potential of the transition metal complexes

The desired 'ballpark' potential for electrocatalyzed CO_2 reduction ranges from −0.5 V to −1.9 V *vs.* NHE at pH 7, which is a generalization based on the thermodynamic limits of CO_2 reduction *via* PCET mechanisms and the single-election CO_2 reduction potential without a catalyst present. Although nearly all metals from Group 6 to Group 10 have been reported with active catalysts for CO_2 reduction, the catalytic reactions were mediated with very different ligand sets and at different redox cycles as shown in Table 2.

The redox potential of the 3d metal complexes changes significantly across the periodic table as shown in Table 3. The redox potential can be strongly related to their chemical reactivity. Fujita and coworkers have shown a close-to-linear relationship between Co(II/I) redox potential and Co(I)–CO_2 affinity in series of cobalt aza-marocyclic complexes.[92] The CO_2 binding affinity generally increases as the metal reduction potential becomes more negative. Similar relationships between hydricity of the $(M - H)^{n+}$ species and the $M^{(n+1)/n}$ redox potentials will also be discussed (see section 6.2). With the tetraphenylporphyrin (TPP) ligand as an example, the metal-based M(III/II) redox potential of 3d metals steadily becomes more positive, spanning ~1.8 V from Cr(III/II) to Ni(III/II).

Table 3 Metal-based redox potentials of 3d metal complexes with 5,10,15,20-Tetraphenylporphin (TPP) ligand *vs.* NHE

	$E(M^{III/II})$/V	$E(M^{II/I})$/V	$E(M^{I/0})$/V	Ref.
$[Cr(TPP)]^+$	−0.61	—	—	93
[Mn(TPP)Cl]	−0.21	—	—	94
[Fe(TPP)Cl]	0.05	−0.80	−1.46	95
[Co(TPP)]	0.84	−0.62	−1.78	22
[Ni(TPP)]	1.25	−1.07	—	96

Potentials are measured for $[Cr(TPP)](ClO_4)$, [Mn(TPP)Cl], [Fe(TPP)Cl], [Co(TPP)] and [Ni(TPP)] in DMF with 0.1 M electrolyte concentrations. The ligand-centered reductions of Cr, Mn and Ni are left out. The conversion from SCE to NHE by +0.24 V is used here.

As for CO_2 reduction, the Fe(I/0) and Co(I/0) redox wave of [Fe(TPP)Cl] and [Co(TPP)] fit well to the expected trend for CO_2 reduction potentials. The reduction potential required to form low-valent species, which is expected to be related to the nucleophilicity of the metal center, is essential to CO_2 activation and reduction. Of course, to accomplish a catalytic cycle involving CO_2 reduction, the binding strength with CO_2 must be balanced with dissociation of product molecules to avoid thermodynamic traps.[97,98]

There are some general trends that are apparent when comparing the electronic structure of transition metal centers.[75] The 4d and 5d transition metals behave similarly with one another in comparison to the 3d transition metals. Moving from left to right, the electronegativity and ionization energy of transition metals increases with group number, while the d-orbital energy and the metal atom size decreases. Similarly, when moving from top to bottom, the 4d and 5d transition metals have greater electronegativity than the 3d metals. The 4d and 5d orbitals are more diffusive (larger atomic radii) and thus can form stronger bonds with ligands as well.

3. Horizontal trends in transition metal complexes for CO_2 reduction

The activity and product selectivity for CO_2 reduction by transition metal electrocatalysts differs significantly from metal to metal with respect to their horizontal positions in the periodic table. For example, [Fe(TPP)Cl] is among the most active electrocatalysts and can achieve TOF up to 10^4 s^{-1} with added Brønsted acids as proton donor.[12] However, [Co(TPP)Cl] shows much lower activity and the analogous Mn porphyrin is not active for electrocatalytic CO_2 reduction.[22,99] Similar trends can be found with aza-macrocyclic complexes like $[Ni(cyclam)]^{2+}$, which show greater selectivity and activity for electrocatalytic CO_2 reduction than the Co-based analogues.[14,25,100]

3.1 Metal–ligand cooperativity

We have summarized frequently reported ligand frameworks of 3d metal complexes for CO_2 reduction in recent years in Table 4. The backbones of catalysts are generally comprised of

Table 4 Electrocatalytic CO_2 reduction activity of mononuclear 3d metal complexes with typical ligand frameworks

	Cr	Mn	Fe	Co	Ni	Ref.
Cyclam				✗	✓	14, 25 and 87
aza-macrocycles (HMD, N_4H or N_5)			✓	✓	✓	14, 86 and 101
Porphyrin		✗	✓	✓	✗	12, 102 and 103
qtpy			✓	✓	✓	104 and 105
Pincer (CNC or PCP)		✓			✓	46 and 106
Cp + bidentate ligands			✓	✓		24, 107 and 108
CO + bidentate NHC/py	✓	✓				16, 41 and 109

Notes: "✓" indicate positive reports and "✗" indicate negative reports, when available.

multidentate ligands with neutral donors like N, P or C or strong monodentate ligands like CO. The ligand sets produce coordination topologies where there are labile coordination sites (1 or 2) available for CO_2 binding. Polypyridine, macrocyclic amine/phosphine, porphyrin and pincer types ligands are recurring.

There appear to be some general trends in the ligand types for transition metals from Group 6 to Group 10. Mid transition metals like Group 6 and Group 7 metals have only been demonstrated to be active catalysts with combinations of strong π-accepting ligands like carbon monoxide to this point, while the late transition metals like Group 10 metals tend to be most active when combined with strong σ-donating ligands like macrocyclic amines and polydentate phosphines.

The ligand trends can be rationalized by considering the electronic effects of ligand interactions with the respective metal centers. For early transition metals, the d electron energies are high, especially at low oxidation states. The π-accepting ligands stabilize d orbital energies through π-backbonding. For late transition metal groups, the d orbital energies are much lower. Utilization of σ-donating ligands can help to increase the d orbital energies and thus increase nucleophilicity of the metal centers.[97]

Since CO_2 reduction activity is codependent on the metal and the ligand, the 3d metals are better subjects for discussion since they have been explored more thoroughly at this point. We leave the specific topic of ligand design and related developments for later discussion.

3.2 Oxidation states of CO_2 activation intermediates

For the reported CO_2 reduction catalysts from Group 6 to Group 10, earlier transition metals tend to access lower oxidation states during the CO_2 reduction cycles, as can be seen in Table 2. The trend is evident when comparing the known Group 6, Group 8 and Group 10 catalysts. The oxidation states accessed by Group 6 (Cr, Mo, W) catalysts during CO_2 activation are thought to only involve M(0) (with a non-innocent ligand facilitating $2e^-$ reduction of the complex),[42,43,110] while M(0)/M(I)/M(II) states are accessed by the Group 8 metal catalysts (Fe, Ru, Os),[12,54] and M(I)/M(II)/M(III) are observed for Group 10 (Ni, Pd) catalysts.[13,26,62]

The trend of the decreasing oxidation states from right to left in the periodic table appears to be related to the electron counts in the d orbitals. As shown in the proposed square pyramidal intermediates of Cr, Mn, and Fe catalysts in Fig. 4, population of the d_z^2 orbital is generally found to be essential for activating CO_2 and forming a M–C bond. The high d electron counts in the late transition metals make them better nucleophiles at higher oxidation states when supported by strong σ-donating ligands as discussed above.

This trend can also be interpreted from a isoelectronic perspective: for similar classes of catalysts like M(0)(bpy)$(CO)_4$ (Group 6) and M(I)(bpy)$(CO)_3$X (Group 7), there is an apparent need to generate dianion $[M(0)(bpy^{\bullet\bullet})(CO)_3]^{2-}$ for Group 6 catalysts while a monoanion $[M(0)(bpy^{\bullet})(CO)_3]^-$ suffices for Group 7 catalysts.

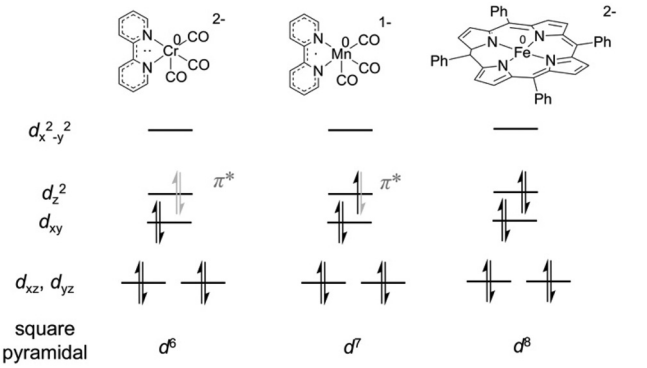

Fig. 4 Electronic structure of metal centers of catalyst from Group 6 to Group 8 for CO_2 reduction to CO. Gray indicates ligand-based electrons of appropriate symmetry to interact with the relevant d orbital.

3.3 A Note on the early transition metals: group 3 to group 5

Grice has recently reviewed the possibility of electrocatalytic CO_2 reduction activity by the early transition metals.[111] CO_2 has been shown to react with Group 3 to Group 5 alkyl or hydrido complexes to generate carboxylates and carbonyl complexes. There are also reports where CO_2 is stoichiometrically or catalytically reduced to methanol, methane *etc*. using Na/Hg amalgam or silanes as reducing agents in the presence of early transition metal complexes.[111] However, molecular complexes from Group 3 to Group 5 have not been reported with significant electrochemical CO_2 reduction activity.[112] Due to their relatively low electronegativities and large atomic radii, early transition metal complexes generally resemble alkali or alkaline earth species, which means they cannot be easily electrochemically reduced and are less likely to form the covalent bonds generally observed in CO_2 reduction intermediates. These qualities must be minimized through ligand design if effective electrocatalysts are to be developed.

4. Vertical trends in transition metal complexes for CO_2 reduction

Moving down the periodic table, the radii of 4d and 5d transition metals are larger than 3d metals and the more diffusive 4d and 5d orbitals form stronger metal–ligand bonds.[75] Consequently, the 4d and 5d transition metal complexes have larger d orbital splitting when coordinated to the same ligand sets as 3d metals. The more polarizable of 4d and 5d transition metals also favor softer ligands like phosphines/NHCs over amines.[113,114]

In general, however, the 4d and 5d transition metal complexes are similar to their 3d counterparts with respect to CO_2 reduction activity. While this could be explained as an isoelectronic effect, the subtle changes in the electronic structures of the analogue complexes can have profound effects on kinetics of CO_2 reduction reactions, indicative of greater mechanistic nuance.

4.1 Isoelectronic metal centers

For Group 6 metals, electrocatalytic CO_2 reduction activity has been demonstrated for all three metals in related ligand frameworks: $Cr(bpy)(CO)_4$, $Mo(^tBu\text{-}bpy)(CO)_4$ and $W(^tBu\text{-}bpy)(CO)_4$.[41,42] Clark *et al.* showed that the bpy ligands in these complexes act as electron reservoirs (as shown in Fig. 4).[42] Recently, Grice and coworkers have shown that the hexacarbonyl complexes $Cr(CO)_6$, $Mo(CO)_6$ and $W(CO)_6$ are capable of performing electrocatalytic CO_2 reduction (which is special for Group 6 metals since Group 7 carbonyls do not have the same activity), albeit at more negative potentials than the bpy-containing compounds.[43] The reported activity of the Cr complexes is lower than for comparable Mo and W complexes by an order of magnitude.[41,43]

For Group 7 metals, both Mn and Re complexes of the formulation *fac*-$M(bpy)(CO)_3X$ (where X is a halide ligand) have shown electrocatalytic CO_2 reduction activity with an extensive modification of the bpy ligands and their bidentate derivatives (Fig. 5).[37,49,115] When Mn is used as a replacement for Re in *fac*-$[M(bpy)(CO)_3X]$ catalysts, there is a decrease in overpotential for Mn complexes over Re, approximately ~300 mV for *fac*-$[Mn(^tBu\text{-}bpy)(CO)_3Br]$ with respect to the Re congener.[17] The TOF_{max} of the two complexes are similar (340 s^{-1} for Mn with 1.4 M TFE as proton donor and 570 s^{-1} for Re with 1.6 M TFE as proton donor).[17] The difference in operating potential appears to originate from a more metal-centered reduction reaction in the Mn complex and corresponding faster rate of halide ligand loss.[116] A large variety of functionalized ligands with bulky and other functional groups, py-NHC, and bidentate NHC ligands have been shown to form active catalysts, often with improved catalytic activity for both Mn and Re.[109,117]

Similar ligand versatility is also observed amongst congeners of Group 8, Group 9 and Group 10. However, systematic studies covering these groups are rare, possibly due to vast activity differences. Among Group 8 metals, there are more similarities between Ru and Os, where both show electrochemical CO_2 reduction with polypyridine ligand sets.[9,30,31,45,118] The Ru complexes of the form $[Ru(bpy)_2(CO)_2]^{2+}$ and $[Ru(tpy)(bpy)(S)]^{2+}$ (S is a solvent molecule, such as MeCN), and the Os complex of $[Os(bpy)_2(CO)(H)]^{2+}$ have all shown CO_2 reduction activity. Ru and Os derivatives of the type $M(bpy)(CO)_2(Cl)_2$ form metallopolymers on the electrode at reducing potentials that are active for CO_2 reduction, although the Os derivative is less efficient.[119–122] In comparison, there is a lack of reported activity for CO_2 reduction by Fe complexes with similar ligand sets, where research on Fe largely focused on porphyrin and other macrocyclic ligands.[86] Fe complexes with qtpy and bpy-based Schiff base-type ligands have only been reported to have CO_2 reduction activity recently.[105,123,124]

For Group 9 metals, complexes of the general form M(Cp)(L)(X) (where L is a bidentate ligand) with Co, Rh and Ir have been all been investigated in the context of electrocatalytic CO_2 reduction.[24,64] This type of complexes have higher reported selectivities for formic acid/formate as a product over CO; $[Co(Cp)(P_2N_2)(MeCN)]^{2+}$, where P_2N_2 is a macrocyclic ligand, demonstrates quantitative yields for formic acid/formate.[24] Cobalt complexes with aza-macrocycle and porphyrin ligands general show selectivity for CO.[14,22,125] Currently, most research on Group 9 catalysts focuses on Co complexes and Ir complexes with pincer ligands; studies on Rh complexes are generally lacking.

For Group 10 metals, Wolf and co-workers have systematically studied the electrochemical CO_2 reduction activity of Ni, Pd and Pt complexes with a series of pincer ligands (PNP or CNC type). The Ni and Pd complexes have shown moderate CO_2 reduction activity, while the Pt complexes have shown more activity towards HER than CO_2 reduction.[126,127]

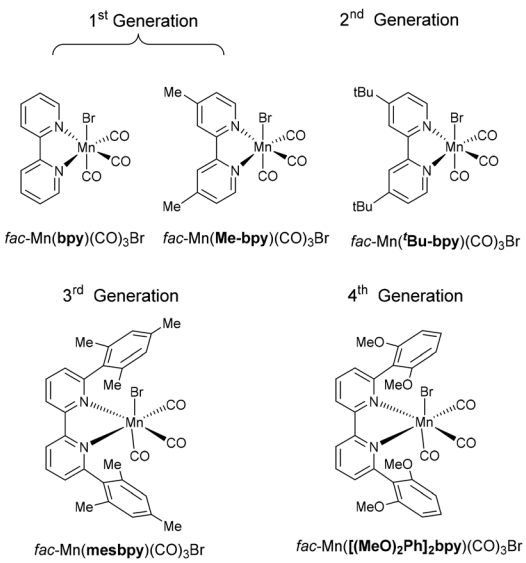

Fig. 5 Summary of the developments of *fac*-$Mn(bpy)(CO)_3X$ catalysts, later designs with bulky groups show increased activity and stability.

4.2 Reaction kinetics influenced by d-orbital energy

As mentioned previously, 4d/5d metals often have stronger metal–ligand interactions than analogous 3d complexes, resulting larger d-orbital splitting. The metal centers in the 4d/5d catalysts are thus more likely to have higher energy unfilled d-orbitals and therefore more difficult to reduce. These types of subtle differences in electronic structure have profound effects on the electrocatalytic reduction of CO_2.

Carter, Kubiak and co-workers have done a series of experimental and theoretical investigations into CO_2 reduction by *fac*-$[Mn(bpy)(CO)_3Br]$ and *fac*-$[Re(bpy)(CO)_3Cl]$ complexes.[35,70,128] As shown in Fig. 6, both the Mn and Re complexes catalyze CO_2 reduction by first activating CO_2 with a doubly reduced radical anion $[M(0)(bpy^{\bullet})(CO)_3]^-$ intermediate (species **3**) to form the hydroxycarbonyl $[M(I)(bpy)(CO)_3(CO_2H)]$ (species **6**), followed by reductive C–O bond cleavage to form carbonyl compound $[M(0)(bpy)(CO)_4]$ (species 2CO) before CO release occurs. This is similar to the previously described CO_2 reduction mechanism involving $[Ru(bpy)_2(CO)_2]^{2+}$ (see Fig. 3).

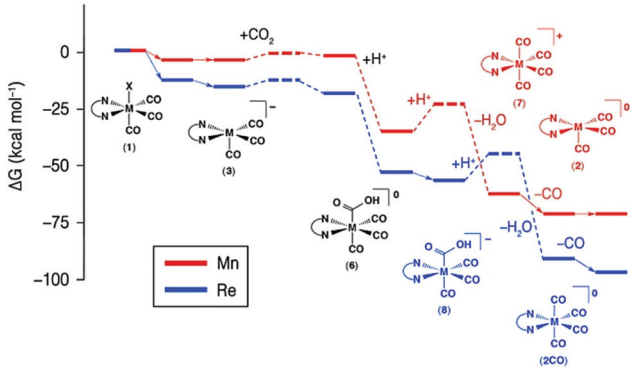

Fig. 6 Potential energy surface of catalytic CO_2 reduction cycle by *fac*-Mn(bpy)$(CO)_3$Br featuring protonation-first path and *fac*-Re(bpy)$(CO)_3$Cl featuring the reduction-first path (at −1.21 and −1.52 V *vs.* NHE for Mn and Re, respectively). Reprinted with permission from *J. Am. Chem. Soc.*, 2014, **136**, 16285–16298. Copyright 2014 American Chemical Society.[70]

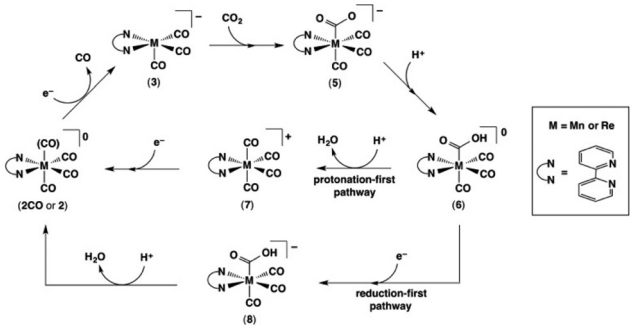

Fig. 7 Protonation-first path and reduction-first path for CO_2 reduction with *fac*-M(bpy)$(CO)_3$X catalyst, where M = Mn and Re. Reprinted with permission from *J. Am. Chem. Soc.*, 2014, **136**, 16285–16298. Copyright 2014 American Chemical Society.[70]

However, the Re catalyst is active at more negative potentials than the corresponding Mn catalyst.

For the Re complex, the energy of the unoccupied d_z^2 orbital (reference to Fig. 4) is predicted to be generally higher than the π^* orbital of the bpy ligand, such that the one-electron reduced $[Re(I)(bpy^{\bullet})(CO)_3Cl]^-$ is relatively stable on the CV timescale requires an additional electron transfer to drive dissociation of the halide ligand and generate the five-coordinate active species $[Re(0)(bpy^{\bullet})(CO)_3]^-$. However, the d_z^2 orbital of the Mn complex is similar in energy to the π^* orbital of the bpy ligand and the halide ligand dissociates readily from $[Mn(I)(bpy^{\bullet})(CO)_3(X)]^-$. With a bulky ligand to prevent dimerization, the $[Mn(0)(bpy^{\bullet})(CO)_3]^-$ active species can be generated at more positive potentials in comparison to $[Re(0)(bpy^{\bullet})(CO)_3]^-$,[17,18,60] consistent with the lower overpotential observed for the Mn catalysts. It is noteworthy that the inhibition of dimerization from the use of bulky bpy ligands results in a two-electron reduction wave for Mn, which is representative of the energy parity for this system relative to Re.[18]

Previous experiments have observed that the Re catalyst can perform CO_2 reduction without an added proton source while the Mn catalysts catalyze CO_2 reduction only with added proton source.[16,89] This observation can also be related to differences in the d orbital electronic structure. Since $[Mn(0)(bpy^{\bullet})(CO)_3]^-$ species can be generated at more positive potentials than Re, the binding affinity between CO_2 and $[Mn(0)(bpy^{\bullet})(CO)_3]^-$ is much weaker than that for $[Re(0)(bpy^{\bullet})(CO)_3]^-$.[17,35,128] Since Mn($\eta^1$-$CO_2$) adduct do not accumulate, CO_2 activation can only be triggered in a concerted way in the presence of a proton donor, which drives reduction and bond cleavage.

Another divergence in the CO_2 reduction mechanism between Mn and Re catalysts that has attracted significant attention is the existence of protonation-first or reduction-first pathways as shown in Fig. 7. For *fac*-M(bpy)$(CO)_3$X catalysts, the formation of the metal carbonyl intermediate from the hydroxycarbonyl intermediate, $[M(I)(bpy)(\eta^1\text{-}COOH)(CO)_3]$, can proceed *via* a protonation-first pathway or a reduction-first pathway for the cleavage of the C–OH bond. The difference between the two pathways is the involvement a M(I) species in the protonation-first pathway and M(0) species in the reduction-first pathway. The protonation-first pathway can proceed at more positive potentials since the following electron transfer would be easier to a cationic species for purely electrostatic reasons.

For the Mn complexes, both the protonation-first path and the reduction-first path have been shown to be viable pathways experimentally and computationally.[60,61] However, the Re analogue generally accesses the reduction-first pathway because of the reduction potential required to generate the $[Re(bpy^{\bullet})(CO)_3]^-$ active species. Modification of the bpy ligand framework on the Re complex with charged imidazolium or thiourea groups has resulted in a decreased barrier for halide loss, but there is no experimental evidence of the Re catalyst participating in the protonation-first pathway at this point.[36,129]

Aside from the similar activity observed for Group 6 and Group 7 metal complexes, there are few cases where 3d/4d/5d metal complexes in single group are reported to have similar activity toward CO_2 reduction. This could be related to much larger electronic structure differences in late transition metals going down the group.

5. Ligand design and evolution for CO_2 reduction

It is important to reiterate that for each catalyst, the metal–ligand interactions are vital to mechanisms for CO_2 reduction and that modification of the ligand framework can lead to orders of magnitude changes in activity.[17,19,21,60] Electrocatalytic CO_2 reduction reactions are very demanding on the ligand framework: the catalyst needs to have high affinity to the substrate (CO_2) while having low affinity to the products (usually CO or $HCOOH/HCOO^-$). The ligand frameworks also need to form stable interactions with the metal

centers across different oxidation states, in order to prevent deleterious demetallation and catalyst polymerization.[6,88,130]

Early studies of electrocatalysts for CO_2 reduction have been focused on finding the right metal complexes with CO_2 reduction activity. In the past decade, with a better understanding of the possible CO_2 reduction mechanisms, more sophisticated ligand design principles have developed.[49,59,74,131] Using redox non-innocent ligands to reduce the catalytic overpotential, synthetic ligand modification strategies to favor specific catalytic routes, and the use of secondary-sphere effects to break scaling relationships have all proven to be effective.[32,49,59]

5.1 Redox non-innocent ligands

Initial molecular electrocatalyst development for CO_2 reduction was largely focused on noble metal complexes because of their propensity to undergo $2e^-$ redox reactions (M(0/II), M(I/III) or M(II/IV)), as is commonly observed in oxidative addition (OA) and reductive elimination (RE) reactions.[5,132] In electrochemistry, the consecutive injection of electrons into a transition metal center inevitably leads to increasingly negative reduction potentials at each step, as the reduction reaction will become less energetically favorable as valency decreases at the metal center.

In transition metal complexes with aromatic type ligands, however, both the vacant d orbitals on the metal center and the π^* orbital on the ligands are available to accept electrons because of their respective contributions to the frontier molecular orbitals of the overall complex. A common example is the *fac*-[Re(bpy)(CO)$_3$Cl] catalyst, where the bpy ligand is redox "non-innocent", as shown in Scheme 2.[10]

Rather than accessing the Re(0/-I) reduction wave, two sequential $1e^-$ reductions of the Re catalyst (which are only ~0.25 V apart) generate the catalytically active [Re(0)(bpy$^{\bullet}$)(CO)$_3$]$^-$ species, which contains a bpy radical anion.[10,128] Similar non-innocent ligand behavior has been discussed for the porphyrin ligand in the [Fe(0)(TPP)]$^{2-}$ active state and also the pyridyldiimine moiety in [Co(N$_4$H)] and other related catalyst platforms.[12,86,133] The use of redox non-innocent ligands greatly influences the applied reduction potential needed for transition metal complexes to initiate CO_2 reduction.

5.2 Strategic ligand design for mechanistic tuning

Strategic ligand designs are often adopted to avoid thermodynamic and kinetic traps in catalytic steps, or to access new reaction pathways requiring lower overpotential. For example, for the *fac*-Mn(bpy)(CO)$_3$Br precatalyst, the initially generated [Mn(0)(bpy)(CO)$_3$]^0 intermediate dimerizes to form a Mn–Mn bond that requires reduction at more negative potentials to cleave before CO_2 reduction can occur.[17] Kubiak and coworkers have explored the use of alkyl functional groups in *fac*-Mn(bpy)(CO)$_3$Br catalysts to facilitate CO_2 reduction. In the *fac*-Mn(^{t}Bu-bpy)(CO)$_3$Br catalysts discussed above, although ^{t}Bu groups did not prevent the dimerization, the *fac*-Mn(^{t}Bu-bpy)(CO)$_3$Br electrocatalyst displays increased catalytic activity at 340 s^{-1} with 1.4 M TFE as proton source, approximately ~300 times faster than the unfunctionalized bpy ligand.[7,17] The incorporation of mesityl groups at the 6,6 positions of the bpy ligand did prevent metal–metal dimerization.[18] The ligand and metal reduction waves of *fac*-[Mn(mesbpy)(CO)$_3$X] merge into a single $2e^-$ wave and the activity was further improved to 5×10^3 s^{-1} with 1.4 M TFE.[18,60] More recently, the introduction of methoxy groups on the mesityl rings by Rochford and coworkers in the catalyst *fac*-([Mn(MeO)$_2$Ph]$_2$bpy)(CO)$_3$Br, resulted in even higher activity and a dramatic reduction of the CO_2 reduction potential by 550 mV by accessing the protonation-first mechanism in the presence of a sufficiently strong Brønsted acid.[61]

Similar mechanistic changes tuned by strategic ligand design have also been reported by Ott and coworkers in [Ru(tpy)(bpy)(S)]$^{2+}$ type of catalysts.[32,134] By selectively introducing steric clash between the tpy and bpy ligands utilizing methyl groups; this change was enough to shift from an *EEC* CO_2 reduction mechanism to an *ECE* mechanism as shown in Scheme 3.

The methyl group position changes on the bpy ligand improved the operating potential for CO_2 reduction by

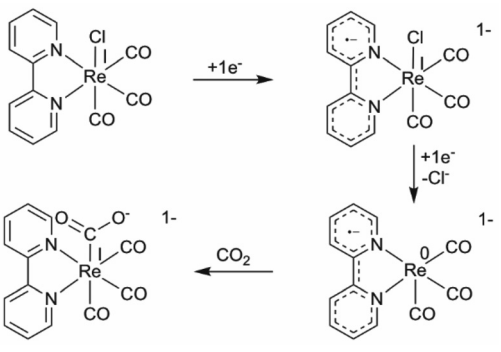

Scheme 2 Involvement of bpy radical anions in CO_2 reduction by *fac*-Mn(bpy)(CO)$_3$X catalysts.

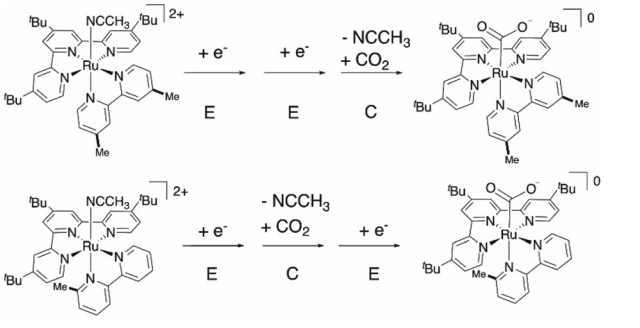

Scheme 3 Activation of CO_2 through a lower overpotential reduction mechanism by accessing *ECE* instead of an *EEC* mechanism in a [Ru(tpy)(bpy)(MeCN)]$^{2+}$-type catalyst. Adapted with permission from ref. 32. Copyright 2015, John Wiley and Sons.[32]

~400 mV. Similar effects have been achieved by replacing the bpy ligand with a phosphine–pyridine ligand, where the phosphine occupies the position *trans* to the solvent ligand.[63]

5.3 Breaking scaling relationship with secondary-sphere effects

Effective strategies for enhancing activity in mononuclear electrocatalysts were also explored using secondary-sphere effects, including installation of pendent proton groups and positively charged groups in the secondary-coordination sphere of the ligand framework.[72,131] This strategy can access new regimes of activity compared to traditional catalyst modification of electronic structure tuning through induction effects. Catalytic enhancement from induction effects is restricted by scaling relationships at the metal center, as electronic changes alter the favorability of substrate binding and product release simultaneously.[98,135]

Savéant and co-workers have shown the limits of electronic structure tuning and the benefits of secondary-sphere effects with systematic modification to [Fe(TPP)Cl] catalysts to enhance catalytic activity.[19–21,72,136] Fig. 8 highlights a few specific examples of relevant derivatives with active-site oriented hydroxy and positively charged ammonium groups. The fluorination of phenyl groups in [Fe(F20TPP)Cl] installs electron-withdrawing substituents on the porphyrin that reduce the required potential for CO_2 reduction. However, the positive shift of the CO_2 reduction potential by 340 mV is accompanied by a drastic decrease of TOF_{max} compared to [Fe(TPP)Cl] due to the relative loss of electron density at the metal center.[136]

The inclusion of hydrogen bond donors at the *ortho*-positions on the *meso*-phenyl groups in [Fe(CAP)Cl] facilitates the binding of CO_2 and also promotes C–O bond cleavage.[19] The stabilization of the one-electron reduced CO_2 as shown in Fig. 9 by hydrogen bonding from the pendent proton groups has been studied extensively.[54,72,83,129,137,138] The installation of these pendent protons is as effective as the theoretical inclusion of 150 M of phenol as the proton donor in solution, with a positive shift of 100 mV in the CO_2 reduction potential and an order of magnitude increase in TOF_{max} (1.6×10^6 s^{-1}) compared to [Fe(TPP)Cl] are observed.

The introduction of four positively charged trimethylanilinium groups in the *para*-position or *ortho*-position ([Fe(*o*-TMAP)Cl]$^{4+}$ and [Fe(*p*-TMAP)Cl]$^{4+}$) of the *meso*-phenyl rings both led to an increase in the observed CO_2 reduction activity. The [Fe(*o*-TMAP)Cl]$^{4+}$ catalyst is especially active, with TOF_{max} on the order 10^6 s^{-1} and a positive shift of 480 mV in CO_2 reduction potentials compared to [Fe(TPP)Cl],[21] which points to specific positional effects and the possibility of a different operative mechanism.

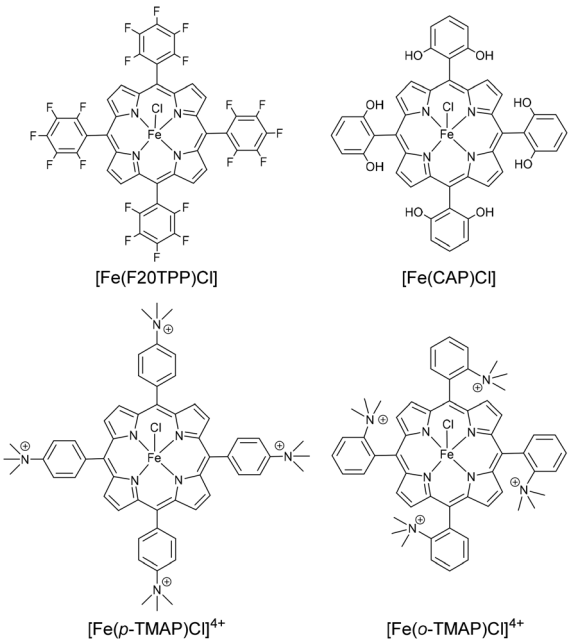

Fig. 8 Development of the porphyrin ligands in [Fe(TPP)Cl] catalysts for improved electrocatalytic activity and overpotential by inductive and secondary-sphere effects.

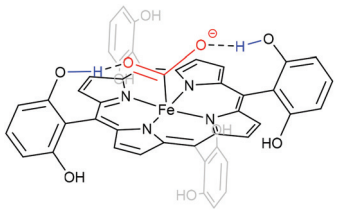

Fig. 9 CO_2 adducts stabilized with pendent protons on the ligand framework of [Fe(CAP)]. Adapted with permission from *J. Am. Chem. Soc.*, 2014, **136**, 11821–11829. Copyright 2014, American Chemical Society.[72]

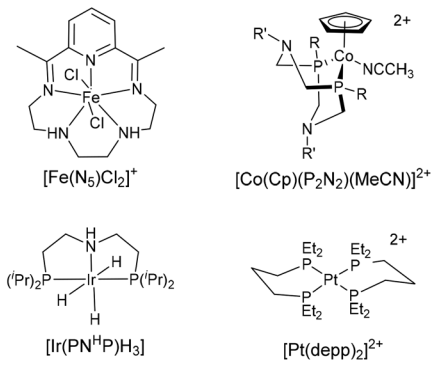

Fig. 10 Representative electrocatalysts for $HCOOH/HCOO^-$ production.

6. Formic acid-producing catalysts

In comparison to CO producing catalysts, there are fewer $HCOOH/HCOO^-$ producing catalysts. Most of electrocatalysts reducing CO_2 to $HCOOH/HCOO^-$ contain late transition metals like Fe,[86,123,124] Co,[24] Ni,[85] Ru,[118] Ir[38,39,139] and Pt,[47] with a few prominent examples shown in Fig. 10. In formate producing catalysts, the influence of the electronic structure of the metal center still exists in the context of intermediate

metal hydride species. Importantly, reactivity and redox potential relationships are commonly reported for the $M–H^{(n+2)+}$ species involved in catalytic formate generation.

Formic acid is a liquid product and could potentially be more desireable than CO. Thus, there is strong interest for designing efficient and active formic acid/formate-producing catalysts.[6] Since electrochemical $HCOOH/HCOO^-$ production is a "two-step" reaction as shown in Scheme 4, the catalyst needs to have the right selectivity on two reaction steps, *i.e.* metal hydride formation over CO_2 binding at the first step and hydride transfer to CO_2 (or CO_2 insertion into the M–H bond) over H_2 evolution in the second step.

Among these $HCOOH/HCOO^-$ producing catalysts, there are complexes which are very selective for formate generation (>90%) and complexes that produce mixed products of $HCOOH/HCOO^-$ with CO and H_2.[140] Cobalt-based complexes with pendent amines of the general type $[Co(Cp)(P_2N_2)(MeCN)]^{2+}$ and iridium complexes with pincer ligands, $[Ir(PN^HP)H_3]$ and $[Ir(PCP)(MeCN)_2H]^+$ (Fig. 1) have shown notable selectivity for the electrocatalytic reduction of CO_2 to $HCOOH/HCOO^-$.

6.1 CO_2 binding *vs.* H^+ binding

The selectivity of the first step reaction in formate generation, *i.e.* the preference of the reduced metal complex for either CO_2 or to H^+, is significantly less discussed compared to the second step, where selectivity between hydride protonation and the activation of CO_2 is important. There have been several computational studies, notably for the CO selective catalysts *fac*-$[Re(bpy)(CO)_3Cl]$ and $[Ni(cyclam)]^{2+}$.[62,128] In both cases, CO_2 binding at the metal center is more thermodynamically favoured than the H^+ binding under experimental conditions, though the latter is dependent on the pK_a of the proton source. For $[Re(0)(bpy^{\bullet})(CO)_3]^-$, it is believed that having extra electron density on the redox non-innocent ligand favours CO_2 binding because of the π symmetry of the CO_2 frontier orbitals.[128] Radiolysis experiments with $[Ni(cyclam)]^{2+}$ show that $[Ni(I)(cyclam)]^+$ has similar reaction rates towards CO_2 and H^+, yet the concentration of CO_2 is much higher than H^+ in neutral water solution, driving selectivity.[141]

Secondary-sphere effects are also believed to have a strong influence on the kinetic parameters of metal hydride formation. In the example of $[Co(Cp)(P_2N_2)(MeCN)]^{2+}$, the pendent amine is proposed to act as H^+ shuttle that facilitates the formation of a Co(II)–H species.[24] Ligand-assisted CO_2 hydrogenation through hydrogen bonding has specifically been demonstrated in the Ir catalyst $[Ir(PN^HP)H_3]$.[139]

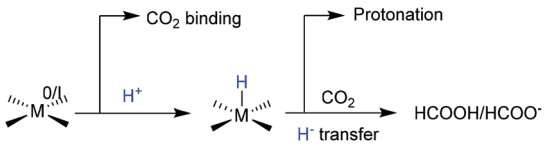

Scheme 4 Generic diagram illustrating the two-step selectivity required for formate production.

6.2 Influence of hydricity on formate generation

Wiedner *et al.*, Waldie *et al.* and Ceballos *et al.* have all recently reviewed the relationship between redox potentials of transition metal complexes and the hydricity of corresponding metal hydrides (or H^- donating ability, defined as ΔG_{H^-}).[47,81,142] These studies have also examined the influence of hydricity on hydride transfer to CO_2, which primarily concerns the second step of the formate generation reaction.[47,81,142]

The hydricity of transition metal hydrides spans a large range (>50 kcal mol^{-1}) from more acid-like H^+ donors to more base-like H^- donors.[81] However, a general linear relationship exists between ΔG_{H^-} and the redox potential of the metal complexes, such that the hydricity of $(M–H)^+$ is related to the $M^{II/I}$ redox potential. As exemplified by the Group 10 metal complexes with diphosphine ligands in Table 5, the metal centers of 4d/5d complexes are harder to reduce than the 3d complexes with the same ligand set. The 4d/5d metal hydrides are also usually stronger hydride donors. This has been successfully exploited by Ceballos *et al.* to perform electrochemical

Table 5 Redox potentials for the $M^{II/I}$, $M^{I/0}$ reductions of select Group 10 metal complexes with diposphine ligands and their corresponding hydricities and pK_as of $(M – H)^+$. Values are taken in acetonitrile. Ref (Waldie *et al.* 2018)[81]

Complex	$E(M^{II/I})$/V *vs.* $Fc^{+/0}$	$E(M^{I/0})$/V *vs.* $Fc^{+/0}$	Hydricity (kcal mol^{-1})	pK_a
$[Ni(depp)_2]^{2+}$	−0.61	−1.34	66.7	23.3
$[Pd(depp)_2]^{2+}$	−1.22	−1.22	54.6	22.9
$[Pt(depp)_2]^{2+}$	−1.4	−1.4	53.7	
$[Ni(dmpp)_2]^{2+}$	−0.89	−1.33	60.9	23.9
$[Pt(dmpp)_2]^{2+}$	−1.53	−1.53	50.6	30.4
$[Ni(dppe)_2]^{2+}$	−0.70	−0.88	62.8	14.4
$[Pt(dppe)_2]^{2+}$	−1.24	−1.24	52.8	22.3
$[Ni(dmpe)_2]^{2+}$	−1.39	−1.39	49.3	24.3
$[Pt(dmpe)_2]^{2+}$	−1.73	−1.73	41.8	31.1

depp, 1,3-bis(diphenylphosphino)propane, dmpp, 1,3-bis(dimethylphosphino)propane, dppe, 1,2-bis(diphenylphosphino)ethane, dmpe, 1,2-bis(dimethylphosphino)ethane.

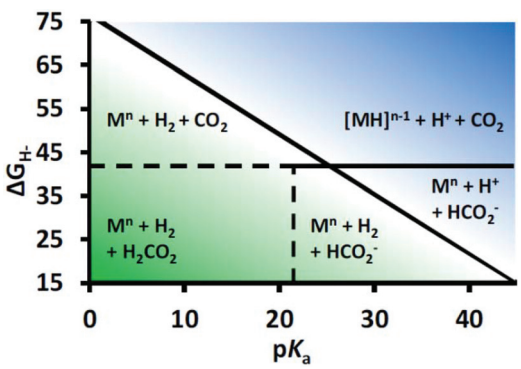

Fig. 11 Free energy diagram for H_2 and HCO_2^- generation comparing the hydricity of the metal hydride (ΔG_{H^-}, in kcal mol^{-1}) and the pK_a of the Brønsted acid. Adapted with permission from *Proc. Natl. Acad. Sci.*, 2018, **115**, 12686–12691. Copyright 2018 National Academy of Sciences.[47]

formate generation with the $[Pt(depp)_2]^{2+}$ complexes, while the analogous $[Ni(depp)_2]^{2+}$ does not show similar activity.[47]

A more general relationship between the hydricity of metal hydrides and the pK_a of the proton source is shown in a Pourbaix-type diagram in Fig. 11. Only metal hydrides that have similar or lower hydricity (more negative ΔG_{H^-}) than formate (44 kcal mol^{-1} in acetonitrile) would be able to perform H^- transfer to CO_2. Considering that the free energy of HER is dependent on pK_a but hydride transfer to CO_2 is not, selective formate generation is often successfully conducted with weak Brønsted acids to inhibit hydride protonation.

7. Conclusions and prospects

In contrast to the behavior of heterogenous CO_2 electrocatalysts of transition metals and alloys,[98,143] periodic trends in molecular electrocatalysts for CO_2 reduction are not as well-defined. In transition metal complexes, catalytic properties have been regularly studied and described on a metal-by-metal or ligand-by-ligand basis. The CO_2 reduction activity of transition metal complexes is strongly influenced by both the metal center and the ligand design. In particular, secondary-sphere effects have been more widely adopted for efficient CO_2 binding and activation, which ultimately resembles the "bifunctional" or multisite activation pathways favored by metalloenzymes.

There are periodic trend observations worth mentioning when analyzing the transition metal molecular electrocatalysts for CO_2 reduction in groups. The activity trends, which are largely derived from the d electron counts, redox properties, and electronic structure shifts, can be described horizontally and vertically.

Horizontal trends:

1. The mid transition metals (like Cr and Mn) favor strong π-accepting ligands and late transition metals (like Ni) favor strong σ-donating ligand for CO_2 activation.

2. The oxidation state achieved by a transition metal catalyst during CO_2 reduction cycles generally increases across the periodic table.

3. Late transition metals appear to afford both CO and formate production catalysts while mid transition metal only show activity toward CO production.

Vertical trends:

1. 3d, 4d and 5d metal complexes in the same group show similar CO_2 reduction activity where the metal centers display "isoelectronic" effects. However, this is more applicable with mid-transition metals than late transition metals.

2. Stronger metal–ligand interactions lead to increasing d orbital splitting and more negative working potentials for the 4d and 5d metal complexes.

There are continuing challenges for electrocatalytic CO_2 reduction with homogenous catalysts. As of now, the best reported molecular electrocatalysts for CO_2 reduction have not shown stability for more than a few days.[142] Also, there has not yet been a breakthrough in our understanding of how to consistently achieve multielectron reduced products beyond the paradigmatic CO or HCOOH. The development of the next generation of CO_2 reduction catalysts will require combined, multidisciplinary efforts focused on understanding these effects and their consequences to challenge the generality of the trends summarized here.

Abbreviations

bpy	2,2′-Bipyridine
Cp	Cyclopentadienyl
Cp*	Pentamethyl-cyclopentadienyl
cyclam	1,4,8,11-Tetraazacyclotetradecane
MeCN	Acetonitrile
NHC	N-heterocyclic carbene
^{t}Bu-	*tert*-Butyl
TFE	Trifluoroethanol
TPP	5,10,15,20-Tetraphenylporphin
tpy	2,2′:6′2″-Terpyridine
qtpy	2,2:6′,2″:6″,2″-Quaterpyridine
triphos	Triphosphine
py	Pyridine

Conflicts of interest

There are no conflicts to declare.

Notes and references

1 P. M. Cox, R. A. Betts, C. D. Jones, S. A. Spall and I. J. Totterdell, *Nature*, 2000, **408**, 184–187.
2 S. Solomon, G.-K. Plattner, R. Knutti and P. Friedlingstein, *Proc. Natl. Acad. Sci. U. S. A.*, 2009, **106**, 1704–1709.
3 M. Mikkelsen, M. Jørgensen and F. C. Krebs, *Energy Environ. Sci.*, 2010, **3**, 43–81.
4 BP p.l.c., BP Statistical Review of World Energy 67th Edition, 2018.
5 M. Rakowski Dubois and D. L. Dubois, *Acc. Chem. Res.*, 2009, **42**, 1974–1982.
6 E. E. Benson, C. P. Kubiak, A. J. Sathrum and J. M. Smieja, *Chem. Soc. Rev.*, 2009, **38**, 89–99.
7 H. Takeda, C. Cometto, O. Ishitani and M. Robert, *ACS Catal.*, 2017, **7**, 70–88.
8 R. Francke, B. Schille and M. Roemelt, *Chem. Rev.*, 2018, **118**, 4631–4701.
9 H. Ishida, K. Tanaka and T. Tanaka, *Organometallics*, 1987, **6**, 181–186.
10 B. P. Sullivan, C. M. Bolinger, D. Conrad, W. J. Vining and T. J. Meyer, *J. Chem. Soc., Chem. Commun.*, 1985, 1414–1416.
11 D. L. DuBois and A. Miedaner, *J. Am. Chem. Soc.*, 1987, **109**, 113–117.

12 I. Bhugun, D. Lexa and J.-M. Savéant, *J. Am. Chem. Soc.*, 1996, **118**, 1769–1776.
13 M. Beley, J. P. Collin, R. Ruppert and J. P. Sauvage, *J. Am. Chem. Soc.*, 1986, **108**, 7461–7467.
14 B. J. Fisher and R. Eisenberg, *J. Am. Chem. Soc.*, 1980, **102**, 7361–7363.
15 M. Hammouche, D. Lexa, M. Momenteau and J. M. Saveant, *J. Am. Chem. Soc.*, 1991, **113**, 8455–8466.
16 M. Bourrez, F. Molton, S. Chardon-Noblat and A. Deronzier, *Angew. Chem., Int. Ed.*, 2011, **50**, 9903–9906.
17 J. M. Smieja, M. D. Sampson, K. A. Grice, E. E. Benson, J. D. Froehlich and C. P. Kubiak, *Inorg. Chem.*, 2013, **52**, 2484–2491.
18 M. D. Sampson, A. D. Nguyen, K. A. Grice, C. E. Moore, A. L. Rheingold and C. P. Kubiak, *J. Am. Chem. Soc.*, 2014, **136**, 5460–5471.
19 C. Costentin, S. Drouet, M. Robert and J.-M. Saveant, *Science*, 2012, **338**, 90–94.
20 C. Costentin, M. Robert, J.-M. Savéant and A. Tatin, *Proc. Natl. Acad. Sci. U. S. A.*, 2015, **112**, 6882–6886.
21 I. Azcarate, C. Costentin, M. Robert and J.-M. Savéant, *J. Am. Chem. Soc.*, 2016, **138**, 16639–16644.
22 D. Behar, T. Dhanasekaran, P. Neta, C. M. Hosten, D. Ejeh, P. Hambright and E. Fujita, *J. Phys. Chem. A*, 1998, **102**, 2870–2877.
23 D. C. Lacy, C. C. L. McCrory and J. C. Peters, *Inorg. Chem.*, 2014, **53**, 4980–4988.
24 S. Roy, B. Sharma, J. Pécaut, P. Simon, M. Fontecave, P. D. Tran, E. Derat and V. Artero, *J. Am. Chem. Soc.*, 2017, **139**, 3685–3696.
25 J. Schneider, H. Jia, K. Kobiro, D. E. Cabelli, J. T. Muckerman and E. Fujita, *Energy Environ. Sci.*, 2012, **5**, 9502.
26 J. D. Froehlich and C. P. Kubiak, *J. Am. Chem. Soc.*, 2015, **137**, 3565–3573.
27 Y. Wu, B. Rudshteyn, A. Zhanaidarova, J. D. Froehlich, W. Ding, C. P. Kubiak and V. S. Batista, *ACS Catal.*, 2017, **7**, 5282–5288.
28 J.-W. Wang, H.-H. Huang, J.-K. Sun, D.-C. Zhong and T.-B. Lu, *ACS Catal.*, 2018, **8**, 7612–7620.
29 T. Fogeron, T. K. Todorova, J.-P. Porcher, M. Gomez-Mingot, L.-M. Chamoreau, C. Mellot-Draznieks, Y. Li and M. Fontecave, *ACS Catal.*, 2018, **8**, 2030–2038.
30 Z. Chen, C. Chen, D. R. Weinberg, P. Kang, J. J. Concepcion, D. P. Harrison, M. S. Brookhart and T. J. Meyer, *Chem. Commun.*, 2011, **47**, 12607.
31 C. W. Machan, M. D. Sampson and C. P. Kubiak, *J. Am. Chem. Soc.*, 2015, **137**, 8564–8571.
32 B. A. Johnson, S. Maji, H. Agarwala, T. A. White, E. Mijangos and S. Ott, *Angew. Chem., Int. Ed.*, 2016, **55**, 1825–1829.
33 D. L. DuBois, A. Miedaner and R. C. Haltiwanger, *J. Am. Chem. Soc.*, 1991, **113**, 8753–8764.
34 J. A. Therrien, M. O. Wolf and B. O. Patrick, *Inorg. Chem.*, 2014, **53**, 12962–12972.
35 J. M. Smieja and C. P. Kubiak, *Inorg. Chem.*, 2010, **49**, 9283–9289.
36 S. Sung, D. Kumar, M. Gil-Sepulcre and M. Nippe, *J. Am. Chem. Soc.*, 2017, **139**, 13993–13996.
37 M. L. Clark, P. L. Cheung, M. Lessio, E. A. Carter and C. P. Kubiak, *ACS Catal.*, 2018, **8**, 2021–2029.
38 P. Kang, C. Cheng, Z. Chen, C. K. Schauer, T. J. Meyer and M. Brookhart, *J. Am. Chem. Soc.*, 2012, **134**, 5500–5503.
39 P. Kang, T. J. Meyer and M. Brookhart, *Chem. Sci.*, 2013, **4**, 3497.
40 M. Feller, U. Gellrich, A. Anaby, Y. Diskin-Posner and D. Milstein, *J. Am. Chem. Soc.*, 2016, **138**, 6445–6454.
41 J. Tory, B. Setterfield-Price, R. A. W. Dryfe and F. Hartl, *ChemElectroChem*, 2015, **2**, 213–217.
42 M. L. Clark, K. A. Grice, C. E. Moore, A. L. Rheingold and C. P. Kubiak, *Chem. Sci.*, 2014, **5**, 1894–1900.
43 K. A. Grice and C. Saucedo, *Inorg. Chem.*, 2016, **55**, 6240–6246.
44 C. M. Bolinger, N. Story, B. P. Sullivan and T. J. Meyer, *Inorg. Chem.*, 1988, **27**, 4582–4587.
45 M. R. M. Bruce, E. Megehee, B. P. Sullivan, H. H. Thorp, T. R. O'Toole, A. Downard, J. R. Pugh and T. J. Meyer, *Inorg. Chem.*, 1992, **31**, 4864–4873.
46 J. A. Therrien, M. O. Wolf and B. O. Patrick, *Dalton Trans.*, 2018, **47**, 1827–1840.
47 B. M. Ceballos and J. Y. Yang, *Proc. Natl. Acad. Sci. U. S. A.*, 2018, **115**, 12686–12691.
48 J.-M. Savéant, *Chem. Rev.*, 2008, **108**, 2348–2378.
49 N. Elgrishi, M. B. Chambers, X. Wang and M. Fontecave, *Chem. Soc. Rev.*, 2017, **46**, 761–796.
50 A. M. Appel, J. E. Bercaw, A. B. Bocarsly, H. Dobbek, D. L. DuBois, M. Dupuis, J. G. Ferry, E. Fujita, R. Hille, P. J. A. Kenis, C. A. Kerfeld, R. H. Morris, C. H. F. Peden, A. R. Portis, S. W. Ragsdale, T. B. Rauchfuss, J. N. H. Reek, L. C. Seefeldt, R. K. Thauer and G. L. Waldrop, *Chem. Rev.*, 2013, **113**, 6621–6658.
51 C. Chen, J. F. Khosrowabadi Kotyk and S. W. Sheehan, *Chem*, 2018, **4**, 2571–2586.
52 C. Costentin, G. Passard and J.-M. Savéant, *J. Am. Chem. Soc.*, 2015, **137**, 5461–5467.
53 H. A. Schwarz and R. W. Dodson, *J. Phys. Chem.*, 1989, **93**, 409–414.
54 C. Costentin, S. Drouet, G. Passard, M. Robert and J.-M. Savéant, *J. Am. Chem. Soc.*, 2013, **135**, 9023–9031.
55 A. J. Göttle and M. T. M. Koper, *Chem. Sci.*, 2017, **8**, 458–465.
56 J. Qiao, Y. Liu, F. Hong and J. Zhang, *Chem. Soc. Rev.*, 2014, **43**, 631–675.
57 C. Costentin, S. Drouet, M. Robert and J.-M. Savéant, *J. Am. Chem. Soc.*, 2012, **134**, 11235–11242.
58 A. J. Sathrum and C. P. Kubiak, *J. Phys. Chem. Lett.*, 2011, **2**, 2372–2379.
59 K. D. Vogiatzis, M. V. Polynski, J. K. Kirkland, J. Townsend, A. Hashemi, C. Liu and E. A. Pidko, *Chem. Rev.*, 2019, **119**, 2453–2523.
60 M. D. Sampson and C. P. Kubiak, *J. Am. Chem. Soc.*, 2016, **138**, 1386–1393.

61 K. T. Ngo, M. McKinnon, B. Mahanti, R. Narayanan, D. C. Grills, M. Z. Ertem and J. Rochford, *J. Am. Chem. Soc.*, 2017, **139**, 2604–2618.
62 J. Song, E. L. Klein, F. Neese and S. Ye, *Inorg. Chem.*, 2014, **53**, 7500–7507.
63 S. K. Lee, M. Kondo, G. Nakamura, M. Okamura and S. Masaoka, *Chem. Commun.*, 2018, **54**, 6915–6918.
64 C. Caix, S. Chardon-Noblat and A. Deronzier, *J. Electroanal. Chem.*, 1997, **434**, 163–170.
65 D. L. DuBois, A. Miedaner and R. C. Haltiwanger, *J. Am. Chem. Soc.*, 1991, **113**, 8753–8764.
66 P. R. Bernatis, A. Miedaner, R. C. Haltiwanger and D. L. DuBois, *Organometallics*, 1994, **13**, 4835–4843.
67 A. Miedaner, B. C. Noll and D. L. DuBois, *Organometallics*, 1997, **16**, 5779–5791.
68 E. E. Benson, M. D. Sampson, K. A. Grice, J. M. Smieja, J. D. Froehlich, D. Friebel, J. A. Keith, E. A. Carter, A. Nilsson and C. P. Kubiak, *Angew. Chem., Int. Ed.*, 2013, **52**, 4841–4844.
69 Y. Kou, Y. Nabetani, D. Masui, T. Shimada, S. Takagi, H. Tachibana and H. Inoue, *J. Am. Chem. Soc.*, 2014, **136**, 6021–6030.
70 C. Riplinger, M. D. Sampson, A. M. Ritzmann, C. P. Kubiak and E. A. Carter, *J. Am. Chem. Soc.*, 2014, **136**, 16285–16298.
71 I. Osadchuk, T. Tamm and M. S. G. Ahlquist, *ACS Catal.*, 2016, **6**, 3834–3839.
72 C. Costentin, G. Passard, M. Robert and J.-M. Savéant, *J. Am. Chem. Soc.*, 2014, **136**, 11821–11829.
73 C. Römelt, J. Song, M. Tarrago, J. A. Rees, M. van Gastel, T. Weyhermüller, S. DeBeer, E. Bill, F. Neese and S. Ye, *Inorg. Chem.*, 2017, **56**, 4745–4750.
74 C. Costentin, J.-M. Savéant and C. Tard, *Proc. Natl. Acad. Sci. U. S. A.*, 2018, **115**, 9104–9109.
75 J. F. Hartwig, *Organotransition metal chemistry: from bonding to catalysis*, University Science Books, Mill Valley, California, 2010.
76 M. Aresta, A. Dibenedetto and E. Quaranta, *Reaction Mechanisms in Carbon Dioxide Conversion*, Springer, Berlin, Heidelberg, 2016.
77 L. G. Dodson, M. C. Thompson and J. M. Weber, *Annu. Rev. Phys. Chem.*, 2018, **69**, 231–252.
78 J. Costamagna, *Coord. Chem. Rev.*, 1996, **148**, 221–248.
79 D. H. Gibson, *Coord. Chem. Rev.*, 1999, **185–186**, 335–355.
80 X. Yin and J. R. Moss, *Coord. Chem. Rev.*, 1999, **181**, 27–59.
81 K. M. Waldie, A. L. Ostericher, M. H. Reineke, A. F. Sasayama and C. P. Kubiak, *ACS Catal.*, 2018, **8**, 1313–1324.
82 K. Kobayashi and K. Tanaka, *Inorg. Chem.*, 2015, **54**, 5085–5095.
83 K. Kobayashi and K. Tanaka, *Phys. Chem. Chem. Phys.*, 2014, **16**, 2240.
84 F. J. Fernández-Alvarez, M. Iglesias, L. A. Oro and V. Polo, *ChemCatChem*, 2013, **5**, 3481–3494.
85 J. P. Collin, A. Jouaiti and J. P. Sauvage, *Inorg. Chem.*, 1988, **27**, 1986–1990.
86 L. Chen, Z. Guo, X.-G. Wei, C. Gallenkamp, J. Bonin, E. Anxolabéhère-Mallart, K.-C. Lau, T.-C. Lau and M. Robert, *J. Am. Chem. Soc.*, 2015, **137**, 10918–10921.
87 M. Beley, J.-P. Collin, R. Ruppert and J.-P. Sauvage, *J. Chem. Soc., Chem. Commun.*, 1984, 1315.
88 R. H. Crabtree, *Chem. Rev.*, 2015, **115**, 127–150.
89 J. Hawecker, J.-M. Lehn and R. Ziessel, *J. Chem. Soc., Chem. Commun.*, 1984, 328–330.
90 M. L. Pegis, J. A. S. Roberts, D. J. Wasylenko, E. A. Mader, A. M. Appel and J. M. Mayer, *Inorg. Chem.*, 2015, **54**, 11883–11888.
91 C. Riplinger and E. A. Carter, *ACS Catal.*, 2015, **5**, 900–908.
92 E. Fujita, C. Creutz, N. Sutin and D. J. Szalda, *J. Am. Chem. Soc.*, 1991, **113**, 343–353.
93 S. L. Kelly and K. M. Kadish, *Inorg. Chem.*, 1984, **23**, 679–687.
94 K. M. Kadish, in *Progress in Inorganic Chemistry*, ed. S. J. Lippard, John Wiley & Sons, Inc., Hoboken, NJ, USA, 1986, vol. 34, pp. 435–605.
95 A. Giraudeau, H. J. Callot, J. Jordan, I. Ezhar and M. Gross, *J. Am. Chem. Soc.*, 1979, **101**, 3857–3862.
96 D. Chang, T. Malinski, A. Ulman and K. M. Kadish, *Inorg. Chem.*, 1984, **23**, 817–824.
97 J. Schneider, H. Jia, J. T. Muckerman and E. Fujita, *Chem. Soc. Rev.*, 2012, **41**, 2036–2051.
98 H. A. Hansen, J. B. Varley, A. A. Peterson and J. K. Nørskov, *J. Phys. Chem. Lett.*, 2013, **4**, 388–392.
99 M. N. Mahmood, D. Masheder and C. J. Harty, *J. Appl. Electrochem.*, 1987, **17**, 1223–1227.
100 J. Honores, D. Quezada, M. García, K. Calfumán, J. P. Muena, M. J. Aguirre, M. C. Arévalo and M. Isaacs, *Green Chem.*, 2017, **19**, 1155–1162.
101 C.-M. Che, S.-T. Mak, W.-O. Lee, K.-W. Fung and T. C. W. Mak, *J. Chem. Soc., Dalton Trans.*, 1988, 2153–2159.
102 K. Takahashi, K. Hiratsuka, H. Sasaki and S. Toshima, *Chem. Lett.*, 1979, **8**, 305–308.
103 J. Shen, R. Kortlever, R. Kas, Y. Y. Birdja, O. Diaz-Morales, Y. Kwon, I. Ledezma-Yanez, K. J. P. Schouten, G. Mul and M. T. M. Koper, *Nat. Commun.*, 2015, **6**, 8177.
104 K.-M. Lam, K.-Y. Wong, S.-M. Yang and C.-M. Che, *J. Chem. Soc., Dalton Trans.*, 1995, 1103–1107.
105 C. Cometto, L. Chen, P.-K. Lo, Z. Guo, K.-C. Lau, E. Anxolabéhère-Mallart, C. Fave, T.-C. Lau and M. Robert, *ACS Catal.*, 2018, **8**, 3411–3417.
106 T. H. T. Myren, A. M. Lilio, C. G. Huntzinger, J. W. Horstman, T. A. Stinson, T. B. Donadt, C. Moore, B. Lama, H. H. Funke and O. R. Luca, *Organometallics*, 2019, **38**, 1248–1253.
107 A. Rosas-Hernández, P. G. Alsabeh, E. Barsch, H. Junge, R. Ludwig and M. Beller, *Chem. Commun.*, 2016, **52**, 8393–8396.
108 E. Oberem, A. F. Roesel, A. Rosas-Hernández, T. Kull, S. Fischer, A. Spannenberg, H. Junge, M. Beller, R. Ludwig, M. Roemelt and R. Francke, *Organometallics*, 2019, **38**, 1236–1247.

109 F. Franco, M. F. Pinto, B. Royo and J. Lloret-Fillol, *Angew. Chem.*, 2018, **130**, 4693–4696.
110 G. Neri, P. M. Donaldson and A. J. Cowan, *J. Am. Chem. Soc.*, 2017, **139**, 13791–13797.
111 K. A. Grice, *Coord. Chem. Rev.*, 2017, **336**, 78–95.
112 K. A. Grice, C. Saucedo, M. A. Sovereign and A. P. Cho, *Electrochim. Acta*, 2016, **218**, 110–118.
113 S. Gonell and A. J. M. Miller, in *Advances in Organometallic Chemistry*, Elsevier, 2018, vol. 70, pp. 1–69.
114 R. H. Crabtree, *The organometallic chemistry of the transition metals*, Wiley, Hoboken, New Jersey, 6th edn, 2014.
115 A. Sinopoli, N. T. La Porte, J. F. Martinez, M. R. Wasielewski and M. Sohail, *Coord. Chem. Rev.*, 2018, **365**, 60–74.
116 D. C. Grills, J. A. Farrington, B. H. Layne, S. V. Lymar, B. A. Mello, J. M. Preses and J. F. Wishart, *J. Am. Chem. Soc.*, 2014, **136**, 5563–5566.
117 C. J. Stanton, J. E. Vandezande, G. F. Majetich, H. F. Schaefer and J. Agarwal, *Inorg. Chem.*, 2016, **55**, 9509–9512.
118 H. Ishida, H. Tanaka, K. Tanaka and T. Tanaka, *J. Chem. Soc., Chem. Commun.*, 1987, 131–132.
119 C. E. Castillo, J. Armstrong, E. Laurila, L. Oresmaa, M. Haukka, J. Chauvin, S. Chardon-Noblat and A. Deronzier, *ChemCatChem*, 2016, **8**, 2667–2677.
120 M.-N. Collomb-Dunand-Sauthier, A. Deronzier and R. Ziessel, *J. Chem. Soc., Chem. Commun.*, 1994, 189–191.
121 M.-N. Collomb-Dunand-Sauthier, A. Deronzier and R. Ziessel, *Inorg. Chem.*, 1994, **33**, 2961–2967.
122 S. Chardon-Noblat, A. Deronzier, R. Ziessel and D. Zsoldos, *J. Electroanal. Chem.*, 1998, **444**, 253–260.
123 S.-N. Pun, W.-H. Chung, K.-M. Lam, P. Guo, P.-H. Chan, K.-Y. Wong, C.-M. Che, T.-Y. Chen and S.-M. Peng, *J. Chem. Soc., Dalton Trans.*, 2002, 575.
124 A. W. Nichols, S. Chatterjee, M. Sabat and C. W. Machan, *Inorg. Chem.*, 2018, **57**, 2111–2121.
125 X.-M. Hu, M. H. Rønne, S. U. Pedersen, T. Skrydstrup and K. Daasbjerg, *Angew. Chem., Int. Ed.*, 2017, **56**, 6468–6472.
126 J. A. Therrien, M. O. Wolf and B. O. Patrick, *Dalton Trans.*, 2018, **47**, 1827–1840.
127 J. A. Therrien and M. O. Wolf, *Inorg. Chem.*, 2017, **56**, 1161–1172.
128 J. A. Keith, K. A. Grice, C. P. Kubiak and E. A. Carter, *J. Am. Chem. Soc.*, 2013, **135**, 15823–15829.
129 E. Haviv, D. Azaiza-Dabbah, R. Carmieli, L. Avram, J. M. L. Martin and R. Neumann, *J. Am. Chem. Soc.*, 2018, **140**, 12451–12456.
130 C. Costentin, M. Robert and J.-M. Savéant, *Acc. Chem. Res.*, 2015, **48**, 2996–3006.
131 C. Costentin and J.-M. Savéant, *Nat. Rev. Chem.*, 2017, **1**, 87.
132 P. Kang, Z. Chen, M. Brookhart and T. J. Meyer, *Top. Catal.*, 2015, **58**, 30–45.
133 M. Zhang, M. El-Roz, H. Frei, J. L. Mendoza-Cortes, M. Head-Gordon, D. C. Lacy and J. C. Peters, *J. Phys. Chem. C*, 2015, **119**, 4645–4654.
134 B. A. Johnson, H. Agarwala, T. A. White, E. Mijangos, S. Maji and S. Ott, *Chem. – Eur. J.*, 2016, **22**, 14870–14880.
135 M. L. Pegis, C. F. Wise, B. Koronkiewicz and J. M. Mayer, *J. Am. Chem. Soc.*, 2017, **139**, 11000–11003.
136 I. Azcarate, C. Costentin, M. Robert and J.-M. Savéant, *J. Phys. Chem. C*, 2016, **120**, 28951–28960.
137 E. M. Nichols, J. S. Derrick, S. K. Nistanaki, P. T. Smith and C. J. Chang, *Chem. Sci.*, 2018, **9**, 2952–2960.
138 J. Bonin, A. Maurin and M. Robert, *Coord. Chem. Rev.*, 2017, **334**, 184–198.
139 S. T. Ahn, E. A. Bielinski, E. M. Lane, Y. Chen, W. H. Bernskoetter, N. Hazari and G. T. R. Palmore, *Chem. Commun.*, 2015, **51**, 5947–5950.
140 A. Taheri and L. A. Berben, *Chem. Commun.*, 2016, **52**, 1768–1777.
141 C. A. Kelly, E. L. Blinn, N. Camaioni, M. D'Angelantonio and Q. G. Mulazzani, *Inorg. Chem.*, 1999, **38**, 1579–1584.
142 Wieder, *et al.*, *Chem. Rev.*, 2016, **116**, 8655–8692.
143 A. J. Medford, A. Vojvodic, J. S. Hummelshøj, J. Voss, F. Abild-Pedersen, F. Studt, T. Bligaard, A. Nilsson and J. K. Nørskov, *J. Catal.*, 2015, **328**, 36–42.